This document contains the draft version of the following paper: Thakur, A., Chowdhury, S., Wang, C., vec, P., Losert, W., and Gupta., S., K., Indirect pushing based automated micromanipulation of biological cells using optical tweezers. International Journal of Robotics Research, first published on May 21, 2014 doi:10.1177/0278364914523690. Readers are encouraged to get the official version from the journals web site or by contacting Dr. Atul Thakur (athakur@iitp.ac.in).

Indirect Pushing Based Automated Micromanipulation of Biological Cells Using Optical Tweezers

Atul Thakur[1], Sagar Chowdhury[2], Petr Švec[2], Chenlu Wang[3], Wolfgang Losert[3], and Satyandra K. Gupta [*2,4]

[1]Department of Mechanical Engineering, Indian Institute of Technology Patna, Patliputra, Bihar, 800013, India
[2]Department of Mechanical Engineering, University of Maryland, College Park, Maryland 20742, USA
[3]Department of Physics, University of Maryland, College Park, Maryland 20742, USA
[4]Department of Mechanical Engineering and the Institute for Systems Research, University of Maryland, College Park, Maryland 20742, USA

August 11, 2014

Abstract

In this paper, we introduce an indirect pushing based technique for automated micromanipulation of biological cells. In indirect pushing, an optically trapped glass bead pushes a freely diffusing intermediate bead that in turn pushes a freely diffusing target cell towards a desired goal. Some cells can undergo significant changes in their behaviors as a result of direct exposure to a laser beam. Indirect pushing eliminates this problem by minimizing the exposure of the cell to the laser beam. We report an automated feedback planning algorithm that combines three motion maneuvers, namely, *push*, *align*, and *backup* for micromanipulation of cells. We have developed a dynamics based simulation model of indirect pushing dynamics and also identified parameters of measurement noise using physical experiments. We present an optimization-based approach for automated tuning of planner parameters to enhance its robustness. Finally, we have tested the developed planner using our optical tweezers physical setup and carried out a detailed analysis of the experimental results. The developed approach can be utilized in biological experiments for studying collective cell migration by accurately arranging the cells in arrays without exposing them to a laser beam.

[*]All correspondence should be addressed to `skgupta@umd.edu`.

Keywords

Optical tweezers, robotic manipulation, automated planning, micromanipulation, indirect pushing, indirect manipulation.

1 Introduction

Recent advancements in robotics have provided a significant boost to many biomedical research applications (Banerjee and Gupta, 2013) such as controlled non-invasive drug delivery (Yim et al., 2013), non-invasive intra-ocular surgery (Bergeles et al., 2010), effective diagnosis (Ergeneman et al., 2012), automated cell injection (Sakaki et al., 2009), etc., where the precision and operational speed are the key performance criteria. The ability to manipulate cells is necessary for many studies of different biological processes such as embryogenesis, wound healing, or metastasis (Vedula et al., 2012; Weijer, 2009; Ingber, 2006), where the cells need to be quickly arranged in arrays to be able to observe their evolving motility. In addition, various biological applications such as cell transport (Wu et al., 2010, 2011; Hu and Sun, 2011), sorting or separation (Xie et al., 2005; Chapin et al., 2006; Gossett et al., 2010), estimation of mechanical properties of cells (Tan et al., 2010), cell-cell interaction (Ashkin and Dziedzic, 1987; McNerney et al., 2010), etc. require accurate and localized micro-manipulation of cells or other living systems. Unfortunately, cell manipulation is mostly achieved manually; hence, the timing and precision of the experiments are significantly compromised, which leads to lower success rate and higher operational time. Moreover, certain micromanipulation operations cannot be achieved manually, which restricts the application scope of the setup. Automating the manipulation process using a robotic technology can overcome these challenges of manual cell manipulation.

Common techniques utilized for cell manipulation include gradient centrifugation (Sims and Anderson, 2008; Tavalaee et al., 2012), micro-fluidic techniques (Bose et al., 2012), micropipette techniques (Zhang et al., 2012; Shojaei-Baghini et al., 2013), magnetic activated cell sorting (Pawashe et al., 2009; Frutiger et al., 2009; Schriebl et al., 2012), etc. For most of the described techniques, a large sample size may be needed. Moreover, precise and localized manipulation of a given cell may not be possible using these techniques.

Nowadays, optical tweezers (OT) are utilized for performing a single cell micromanipulation. One of the notable advantages of OT based micromanipulation is that it can be utilized for exerting a controlled force in the range of 0.1–100 pN on particles of sizes ranging from 10 nm to 10 μm (Neuman and Nagy, 2008). Optical tweezers are thus considered as a useful tool for cell manipulation as many cells belong to this size range.

Cells can be precisely manipulated using optical tweezers but photo-damage is inflicted upon them due to optical trapping (Ashkin and Dziedzic, 1989). The underlying mechanism for photo-damage has been proposed to be due to the creation of reactive chemical species (Liu et al., 1996; Svoboda and Block, 1994), local heating (Liu et al., 1996), two-photon absorption (Konig et al., 1995, 1996), and singlet oxygen through the excitation of a photo-sensitizer (Neuman et al., 1999). It is commonly speculated that trapping using laser at infrared wave length does not significantly inflict photo-damage. Aabo et al., however, experimentally demonstrated that under continuous, as well as pulsed irradiation with 1070 nm infrared laser, the growth rate of Saccharomyces cerevisiae reduces

with an increase of laser power (Aabo et al., 2010). In their experiments, laser exposure of 0.7 mW had an insignificant effect on cell growth, however, at 2.6 mW the cells ceased to grow. In another experimental study, Ayano et al. showed that the growth rate of *E. coli* cell gets adversely affected at a dose of 0.5 J of 1064 nm laser (Ayano et al., 2006). They also showed that cell division capability of *E. coli* gets affected at even lower doses than 0.35 J of 1064 nm laser. Rasmussen et al. found out that pH of both *E. coli* and *Listeria* declined at trapping powers as low as 6 mW (Rasmussen et al., 2008).

Thus, despite of optical tweezers being promising tools for accurate manipulation of cells, the devastating photo-damage due to direct laser exposure hinders its effectiveness in cell micromanipulation. In the past, our group used gripper formations made of dielectric silica beads to grip and transport yeast cells (Koss et al., 2011). The bead formation can be made from biodegradable polymeric microbeads, and thus can be used for targeted drug-cell interaction study (Steager et al., 2013). This gripper formation based technique significantly reduced laser exposure of the gripped cells during transportation as compared with direct trapping. However, direct contact of the target cell with optically trapped beads still lead to some laser exposure due to the cone shape of the optical trap (Koss et al., 2011).

In order to further reduce the laser exposure to the target cell, we propose the use of an intermediate glass bead positioned in between an optically trapped glass bead and the target cell (Wang et al., 2013). The proposed bead formation can be regarded as a non-prehensile robotic manipulator actuated by optical force. Recent advances in the field of user interfaces (such as iPad® applications for optical tweezers control) have proven to be very useful (Leach et al., 2006; Graydon, 2011) in user-guided micromanipulation. However, manual indirect pushing of cells using optically trapped micro-beads is a time consuming process. In particular, manual micromanipulation is difficult to be used effectively due to the inherent instability of the contact points between indirectly pushed beads and the cells.

In this paper, we combine OT technology with an image guided robotic technique to perform cell micromanipulation. In particular, we report a feedback motion planning approach for indirect pushing of cells using the proposed bead formation. The approach is based on three main components, namely, (1) motion simulation of ensemble of particles in the bead formation with sensing and Brownian noise, (2) noise handling based on Kalman filtering (LaValle, 2006), and (3) feedback motion planning for indirect pushing. We also present an automated approach for tuning parameters of the developed feedback planner to deal with different turning angles of the ensemble. We use a genetic algorithm to optimize the parameters to make the feedback planner robust to sensing and motion uncertainties.

This paper builds on our previous demonstration in which we showed the feasibility of the indirect pushing idea (Thakur et al., 2012). We present the following new results.

- We have incorporated trap dynamics into the simulation model of indirect pushing (see Section 4.1). We have used the new model to optimize the parameters of the feedback planner (see Section 5.2) to further improve its robustness. In addition, the new model has also allowed us to improve the Kalman filtering based localization (i.e., the prediction step of the Kalman filter) of the particles.

- We have experimentally observed that beads stick to each other during pushing due to optical as well as Van der Waals forces (Thakur et al., 2012). This sticking

becomes prominent with the presence of cell culture in the solution. The stuck beads are difficult to recognize in the image as their boundaries merge. This leads to a high failure rate of the previously developed micromanipulation technique in experiments. We have developed a new set of maneuvers (see Section 5.1) to make the feedback policy more robust. In particular, we have introduced a backup maneuver to be able to preemptively detach the beads before they start sticking to each other.

We have also developed a new type of the align maneuver. The earlier version of the align maneuver utilized only translation motion to position the effector bead in respect to the intermediate bead. This was highly inefficient, and sometimes the execution of the maneuver interfered with the Brownian motion of the intermediate bead. We have introduced circular motion in the align maneuver which minimizes this interference.

We have introduced new parameters for the maneuvers and optimized them using the simulation based approach as described in the paper. This has significantly enhanced the speed, robustness, and precision of the feedback planner.

- We report an improved method for experimentally determining the measurement noise and dynamics parameters of the indirect pushing model (see Section 4.2).

- We report detailed experimental results with actual yeast cells. In our previous experiments, we used glass beads as surrogates for yeast cells (Thakur et al., 2012). In the new set of experiments, the use of yeast cells has revealed several issues that were not present in the former setup. In particular, detection of a cell is more difficult compared to the detection of a bead in the image. This is because the transparent nature of the cell makes it difficult to detect it in phase contrast imaging in comparison to detecting a bead that has clearly visible outer white annular part. In addition, due to the lower density of the cell and thus its slightly lower mass compared to the silica bead, the cell has increased tendency to transition into a different Z plane during pushing. As a consequence, the image of the cell becomes blurred which prevents the image processing algorithm to reliably recognize it. We have improved the localization technique for predicting the position of the cell and beads using a combination of Hough transform and Kalman filtering (see Section 4.2). The technique utilizes the new model of indirect pushing to significantly improve this prediction.

- Finally, the beads have the same diameter but this may differ for cells. The newly developed feedback planner (see Section 5) allows us to reliably manipulate cells in the range from 4 to 7 μm.

2 Related Work

There is a significant body of literature on pushing-based or non-prehensile manipulation in the area of robotics and we present here some representative research papers. Mason (Mason, 1986) reported a rule-based approach (i.e., an approach based on geometric reasoning and physical parameters such as the coefficient of friction) for determining the rotation direction of an object, which is pushed by a flat fence. Akella and Mason (Akella and Mason, 1992) reported an approach for generation of complete, open loop,

pushing plans which do not require position information. Lynch (Lynch, 1999) proved theorems to characterize polygonal part geometries which can be pushed along any desired trajectory using open loop stable pushing. Rezzoug and Gorce (Rezzoug and Gorce, 1999) presented a two-finger pushing approach using fixed contact points and solved the optimal force distribution problem using a linear programming approach.

Pereira *et al.* (Pereira et al., 2004) addressed the problem of transporting a polygonal object by multiple mobile agents using a combination of pushing and caging operations. Li and Payandeh (Li and Payandeh, 2007) presented a sensor-less manipulation approach for translating and orienting convex objects by a two-agent point-contact push. Igarashi *et al.* (Igarashi et al., 2010) reported a dipole-based local control approach to push objects along a given path using dipole field based approach. Behren *et al.* (Behrens et al., 2010) reported a dynamic model incorporating inertia and friction effects. Kopicki *et al.* (Kopicki et al., 2009) have presented a probabilistic framework for learning and then predicting the motions of interacting rigid bodies in 3D. Cosgun *et al.* (Cosgun et al., 2011) reported a heuristic based planning algorithm for placing convex objects on a cluttered plane such as a table or floor using a sequence of pushing operations.

Recently, Cappelleri *et al.* (Cappelleri et al., 2012) reported an approach for coordinated control of multiple micromanipulators for the use in 2D and 3D micromanipulation tasks using a feature-defined (FD) micro-caging transport primitives. In the micro-caging approach of Cappelleri *et al.* planning is not automated. Landolsi *et al.* (Landolsi et al., 2012) reported nonlinear analysis of pushing based micro-manipulation using Atomic Force Microscope (AFM).

There is a previous work in the area of automated path planning and cell transport using OT. Banerjee *et al.* (Banerjee et al., 2010, 2012) used a partially observable Markov decision process (POMDP) to formulate a path planning problem for OT to deal with the dynamic nature of the environment and solved it using stochastic dynamic programming (SDP). The trapping force for a particle displaced from the focal point of a laser is described in (Banerjee et al., 2009; Hu and Sun, 2011; Bista et al., 2013). Chowdhury *et al.* (Chowdhury et al., 2012b, 2011) developed both decision theoretic based and heuristic planning approach for automated transport of cells inside an optical tweezers assisted microfluidic chamber using direct trapping. Wu *et al.* (Wu et al., 2011) reported an approach based on modified A* based global path planning automated cell transportation using OT. Wu *et al.* used a PI control scheme to adjust motion velocity online in order to maintain a cell within a laser trap. Chen *et al.* (Chen et al., 2013) developed a flocking control algorithm to automatically transport a collection of cells trapped by OT towards a predefined region.

Cells are vulnerable to direct pushing since the light cone of the laser beam overlaps with the trapped cell (Koss et al., 2011). With the six bead indirect gripping approach, the negative effect of the light cone on the cell is avoided (Chowdhury et al., 2012a; Banerjee et al., 2011). Chowdhury *et al.* (Chowdhury et al., 2013, 2012c) developed an A* based approach for automated, indirect transport of cells using different types of gripper formations.

To the best of authors' knowledge, there is no automated micromanipulation technique reported in the OT domain that utilizes *indirect pushing*. Here, *indirect pushing* refers to the process of pushing a cell towards a goal location using a freely diffusing silica bead which is eventually pushed by another optically trapped silica bead. On the other hand, we use the term "indirect transport" in our previous works (Chowdhury et al., 2013,

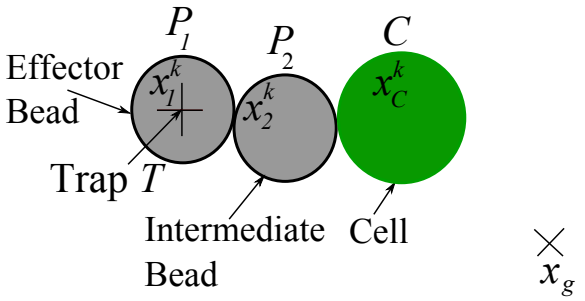

Figure 1: The trap T_1 should be controlled in such a way that it moves the effector bead P_1 to push the intermediate bead P_2 in the bead formation and thereby indirectly pushes the cell C towards the goal x_g.

2012c) to describe the manipulation of a cell using optically trapped silica beads that are in direct contact with the cell. One of the main challenges encountered in the automated pushing-based transport of cells is the uncertainty in the measurement of positions. Most of the reported techniques in the area of pushing-based manipulation do not deal with the sensing noise in position of a bead or cell. In this paper we report a simulation-aided robust pushing-based manipulation technique and present results of experiments of automated transport of yeast cells.

3 Overview

3.1 Problem Statement

Let,

- C be a cell located at x_c^k,
- P_1 be the *effector* bead of the bead formation that is situated at x_1^k and trapped by the optical trap T_1,
- P_2 be the *intermediate* bead of the bead formation that is situated at x_2^k, and
- x_g be the goal location of the cell C.

The task is to compute a feedback plan that determines the motion of the trap for the effector bead to push the intermediate bead P_2, which in turn pushes the cell to its desired goal x_g (see Figure 1). During this process, it is compulsory that P_1 and C do not come in contact.

3.2 Overview of Approach

We adopt the following steps to solve the above task.

(i.) Develop a simulator based on kinematics and dynamics of the indirect pushing operation to simulate the motion of particles in the bead formation, their mutual interactions in terms of collisions and pushing, and the sensing noise.

(ii.) Perform experiments on the physical optical tweezers setup to identify measurement noise.

(iii.) Utilize image processing and Kalman filtering based approach to estimate the positions of P_1, P_2, and C from the video stream obtained by CCD camera.

(iv.) Develop a feedback planner to automatically control the optical trap T_1 that actuates P_1, which thereby pushes P_2 and thus imparts momentum to C to move it towards the goal x_g.

(v.) Utilize optimization based approach to automatically tune parameters of the feedback planner so that the generated plans are robust to different sensor noise and turning angles.

4 Simulation of Indirect Pushing

In this section, we present a kinematic and dynamic model of indirect pushing operation, a simulation of the indirect pushing, and a parameter identification procedure to determine sensor noise from physical experiments.

4.1 Model Description

We have made the following three assumptions in order to build a kinematic and dynamic model of indirect pushing of particles in the bead formation.

(i.) We approximate the cells and glass beads as perfect spheres in the experiments reported in this paper. Each spherical particle is optically trapped using the holographic optical tweezers in 3D. We, however, observed that most cells lie on the bottom surface of the slide. Hence, their transport can be realized in 2D plane. We approximate each spherical particle using a circle in the developed simulator. Since all motions due to the movement of traps occur in the focal plane of the optical tweezers, the described two-dimensional approximation is justified.

(ii.) We assume that the fluid flow around particles is laminar and hence with very low Reynold number.

(iii.) We assume that the cells and beads are perfect rigid bodies, however, in general, cells are not rigid bodies. In this paper, we are dealing with cell transportation, which is a large scale motion of the order of few tens of microns as compared to the cell size (around 5 μm). Small deflections due to the "softness" of the cell wall have negligible effect on such motions. We observed experimentally that yeast cells behave like rigid bodies to an acceptable extent. Thus, for the sake of simplicity of modelling we represent cells using perfect rigid bodies.

Let r_B and r_C be the radii of the circles representing a glass bead in the bead formation and cell, respectively. We represent the positions of the beads P_1, P_2, the cell C, and the trap T by x_1, x_2, x_C, and x_{trap}, respectively. We denote the velocity of the particle P_1 as $v_1 = \dot{x_1}$.

The equation of motion of the particle P_1 due to the influence of trapping force and drag caused by the fluid medium is given by the Equation 1 (Wu et al., 2013).

$$m\ddot{x_1} = F_{trap}(\Delta x) - F_{drag}(\dot{x_1}) \tag{1}$$

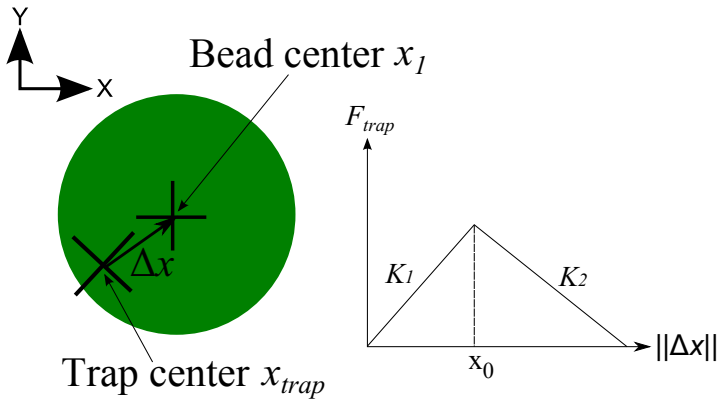

Figure 2: Trapping force model Wu et al. (2013).

In the above equation, m is the mass of P_1, F_{trap} is the trapping force and is given by the Equation 2 (see Figure 2).

$$F_{trap}(\Delta x) = \begin{cases} K_1 \Delta x & 0 < \|\Delta x\| < x_0 \\ -K_2 \Delta x + c & \|\Delta x\| > x_0 \end{cases} \tag{2}$$

Here, $\Delta x = x_1 - x_{trap}$ is the directional vector between the center of the particle P_1 and the trap T, K_1 and K_2 are the trapping stiffness constants that are determined using the method based on (Wu et al., 2013) as described in Section 4.2, and c is a constant. The drag force $F_{drag} = b\dot{x_1}$ is proportional to the particle velocity $\dot{x_1}$. The drag coefficient b is calculated as $b = 6\pi\eta r_B$, where η is the dynamic viscosity of the surrounding fluid medium and r_B is the radius of particle assuming it to be perfectly spherical. In past, Singer *et al.* (Singer et al., 2001) also used similar drag force method to characterize the trapping force on polystyrene beads as large as 10 μm.

In our experiments, the diameter of the beads used is 5 μm while the diameter of the yeast cell varies approximately in the range 5 μm to 10 μm. Also, the maximum speed of these particles is limited by 10 $\frac{\mu m}{s}$. Thus, the Reynold number in case of the beads is very low, which allows to ignore the inertial term $m\ddot{x}$ from Equation 1 (Wu et al., 2013). As a result, Equation 1 can be simplified to Equation 3.

$$F_{trap}(\Delta x) = F_{drag}(\dot{x_1}) \tag{3}$$

In Equation 3, x_1 is varying in continuous time t, i.e., as $x_1(t)$. For convenience of implementation, we discretize time and represent $x_1(t)$ at different discrete time instants using the notation x_1^k, where k denotes a discrete time instant. The speed $v_1^k = \dot{x}_1^k$ of the particle P_1 is determined by Equation 4. This accounts for an optical trap T located at a distance of Δx from the center of the particle.

$$v_1^k = \begin{cases} \frac{K_1}{b} \Delta x & 0 < \Delta x < x_0 \\ \frac{-K_2 \Delta x + c}{b} & \Delta x > x_0 \end{cases} \tag{4}$$

Other particles that are in contact with the moving trapped particle get pushed due to the transfer of momentum. Since we perform pushing actively using image feedback, we can assume direct contact between the pushing and the pushed particle to be maintained as long as the pushed particle keeps moving. This is also ascertained by the fact that due to the viscous medium, the pushed particle stops moving almost instantaneously as soon as its contact with the pushing particle breaks.

The velocity of the particle P_2, imparted by the motion of P_1 is given by v_2^k at the time step k (see Equation (5)).

$$v_2^k = \begin{cases} \xi_b \; max\left(\left\langle v_1^k, \hat{d}_{1,2}\right\rangle, 0\right) \hat{d}_{1,2}, \text{ if } \parallel x_1^k - x_2^k \parallel \leq 2r_B \\ [0,0]^T, \text{ otherwise,} \end{cases} \tag{5}$$

where $\left\langle v_1^k, \hat{d}_{1,2}\right\rangle$ represents dot product of the vectors v_1^k and $\hat{d}_{1,2}$ and $\hat{d}_{1,2} = \frac{x_2^k - x_1^k}{\|x_2^k - x_1^k\|}$ is the unit vector along the normal direction of the contact point between P_1 and P_2. The term $\xi_b = \frac{m}{m_i}$ represents ratio of masses m of the effector bead and m_i of the intermediate bead. Since, the effector and intermediate beads are of same size and material, $m = m_i$ and hence we assume $\xi_b = 1$. The component of momentum along the contact direction $\hat{d}_{1,2}$ is only responsible for translation of P_2. The component of momentum that is normal to the contact direction $\hat{d}_{1,2}$ is responsible for rotational motion, which we can safely ignore in case of cell transport application.

Equation (5) models the pushing action by taking a component of the momentum along the direction of contact. The only component of velocity v_1^k of the pushing bead along $\hat{d}_{1,2}$ is transferred to the pushed particle. Similarly, the velocity of the cell v_C^k at the time instant k is given by Equation (6).

$$v_C^k = \begin{cases} \xi_c \; max\left(\left\langle v_2^k, \hat{d}_{2,C}\right\rangle, 0\right) \hat{d}_{2,C}, \text{ if } \parallel x_C^k - x_2^k \parallel \leq r_B + r_C \\ [0,0]^T, \text{ otherwise,} \end{cases} \tag{6}$$

where $\hat{d}_{2,C} = \frac{x_C^k - x_2^k}{\|x_C^k - x_2^k\|}$ is the unit vector along normal direction of the contact point between P_2 and C. $\xi_c = \frac{m_b}{m_c}$ is the mass ratio between the intermediate bead and the cell where m_b and m_c are the masses of the silica bead and yeast cell, respectively. The mass of the spherical silica bead m_b can be easily determined from the properties of the material. For measuring the mass m_c of the cell we assumed the density of the cell to be similar to water since approximately 70% of the cell is made up by water.

In general, Equations (5) and (6) can be extended to any number of effectors and intermediate beads in the bead formation. However, in this paper, we consider only one effector and intermediate bead for the sake of simplicity. The simulator can also simulate noise due to the measurement errors in addition to the interactions due to collision. We refer to the group of particles P_1, P_2, and C as an *ensemble* for the purpose of description. We introduce some terminology below that is used in this paper.

Ensemble state ($S^k = \left\{x_1^k, x_2^k, x_C^k, x_g^k\right\}$): Ensemble state is defined as a set containing positions of effector bead (P_1), intermediate bead (P_2), cell (C) and goal location x_g at a given discrete time step k.

Action (u^k): An action $u^k = v_1^k$ at a given time step k is the velocity of the trap T_1.

State Transition (F): When a trap moves with velocity $u^k = v_1^k$ at a given time step k, the ensemble transitions from state S^k to S^{k+1} as shown in Equation (7).

$$S^{k+1} = F\left(S^k, u^k\right) \tag{7}$$

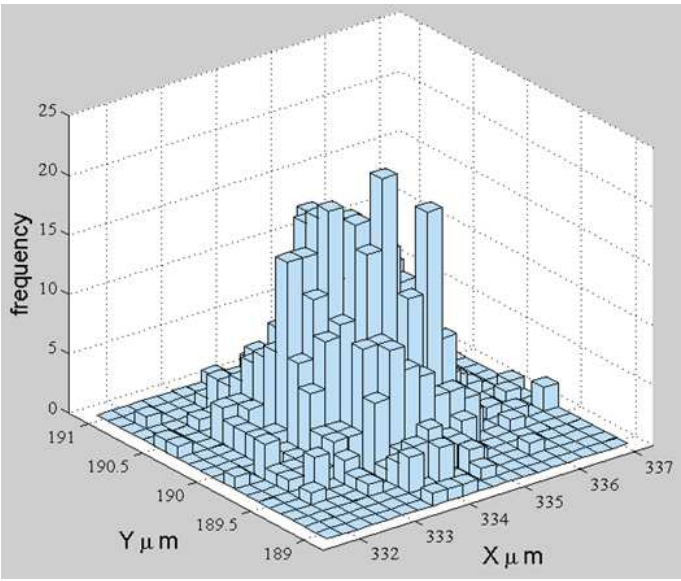

Figure 3: Physical experiment is performed to estimate a noise in the measured position of a trapped bead. The bead is trapped using 8 mW laser power. We record measured positions for 1000 time steps to estimate a covariance matrix of the measurement error.

4.2 System Identification

The positions of particles are measured by processing the video stream captured using a CCD camera in our OT-based experimental setup. We use Hough transform to recognize beads and cells. Due to the variations in the images obtained by the CCD camera, the image processing and feature recognition introduces a measurement noise in position estimation. In addition, Brownian motion of particles introduce process noise. In order to measure the covariance of the measurement error, we trapped a bead with 8 mW laser power and logged the measured position for 1000 time steps. Figure 3 shows the variation of the measured position from the trap location. The measurement noise covariance matrix determined from the data presented in Figure 3 is

$$\Sigma = \begin{pmatrix} 1.06 & 0.45 \\ 0.45 & 0.19 \end{pmatrix}$$

Since the laser power of 8 mW is sufficient to arrest the motion of the bead, the covariance of the measured position can be considered as an estimation of the measurement noise for the purpose of pushing. We utilized a random vector variate drawn from 2-dimensional normal distribution with $[0, 0]^T$ as the mean vector and Σ as the covariance matrix for simulating the measurement noise.

In order to deal with the noise, we utilized Kalman filtering (LaValle, 2006). Based on the assumptions made in Section 4, we limit the maximum speed of the trap to ensure that the trapped particle moves along with the trap. Due to this, a linear model developed in this paper is sufficient for Kalman filtering. In general, for higher speeds, extended Kalman filter can be used with non-linear motion models.

Significant computation time is needed for image processing operations, which may introduce a delay in the execution of a control action. Such delay must be taken into account in the simulator. We logged the time required for image processing for 1000

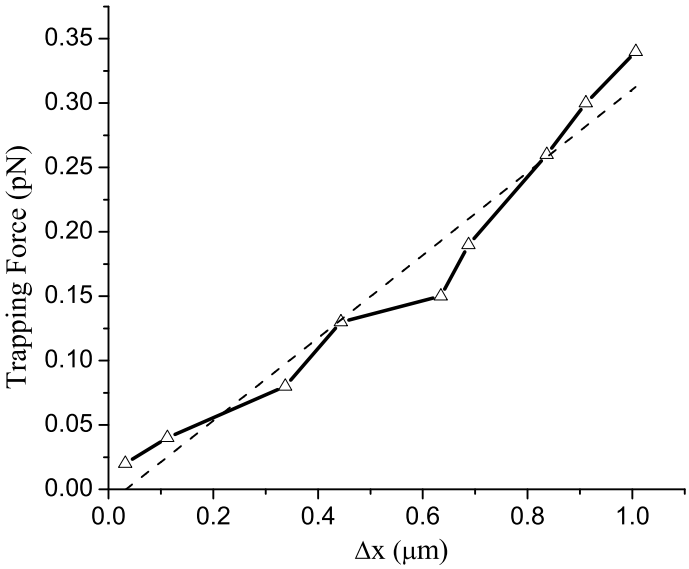

Figure 4: Experimental estimation of the trap stiffness at the trap power of 5.63 mW.

time steps in a physical experiment. We then characterized this computation time as a Gaussian variable with the mean of 0.1 s and standard deviation of 0.04 s. We simulated the image processing time at each control time step by introducing a delay of random time span drawn from a normal distribution with the same mean as well as the standard deviation. Image processing performance largely depends on the processing speed of the computer on which control and planning code is run.

We adjusted the speed of the trap to operate in the region of increasing gradient of the trapping force (see Figure 2), i.e., $\Delta x \leq x_0$. The trapping force gradually decreases beyond x_0, where a particle cannot be reliably trapped. In order to measure the trapping stiffness K_1 in the region of increasing gradient, we programmed the motorized stage that holds the particle to induce a speed on the fluid medium with respect to the laser trap.

In the experiment, we first trapped the particle with a particular laser power and recorded its position. Then we induced a relative speed to the fluid medium by moving the motorized stage with a fixed programmed speed and recorded the final position of the same particle. The induced speed of the fluid medium would try to displace the particle from the trap while trapping force would try to restore it back. Both the forces would reach to the equilibrium at the position Δx apart from the trap location.

From the recorded positions before and after moving the motorized stage, we could compute the displacement Δx of the particle from the trap. The trapping force was measured indirectly by calculating the induced drag force due to moving fluid medium using the drag force equation described in Section 4.1.

In the subsequent round of experiments, we gradually increased the speed of the motorized stage to increase the drag force until the trap was no longer able to hold the particle and recorded the respective Δx. The trapping force is plotted with respective Δx in X-axis. The slope of the plot gives the stiffness of the laser trap K_1 for a particular laser power. From the plot in Figure 4, the trap stiffness K_1 for our operating laser power of 5.3 mW is calculated as 0.3 pN/ μm and x_0 is determined to be 1 μm since beyond this point, the trap cannot stably hold the particle.

5 Local Feedback Planner

In this section, we present a local feedback policy for indirect pushing using the bead formation. The local feedback planner determines a suitable action (i.e., trap motion) to indirectly push the cell towards a desired goal location for any given ensemble state.

5.1 Feedback Policy Algorithm

The feedback policy determines the desired velocity for the trap that moves the effector bead to push the intermediate bead that in turn pushes the cell towards the goal location for any given ensemble state. The main challenges encountered in finding a suitable feedback policy are:

(i.) the contacts between beads and cells do not exist at all times since the contacts may break at any time due to the Brownian motion and the dynamic interaction between the fluid and particles, which leads to nonlinear pushing dynamics, and

(ii.) the measurement uncertainties may lead to an imperfect information about the ensemble state and the existing contacts.

To handle the above described challenges, the feedback policy should be robust to possible instabilities in contacts among the particles. It also should be able to handle the uncertainty in feature recognition of the image processing algorithm. We have developed a feedback policy consisting of three maneuvers to ensure robustness, namely, (1) *push*, (2) *align*, and (3) *backup* (as shown in Figure 5).

The *push* maneuver is activated when the effector and intermediate beads, the cell, and the goal are collinear. This causes the trap T_1 to move the effector bead, which in turn pushes the intermediate bead so that the cell can move towards the goal. Particles may get misaligned due to the dynamics and Brownian motion. As long as the angle between $\hat{d}^k_{2,C}$ and $\hat{d}^k_{1,2}$ is less than a user-specified threshold θ_1 (see Figure 5b), the effector bead, the intermediate bead, and the cell are considered to be aligned. In other words, alignment is detected when $cos^{-1}(\langle \hat{d}^k_{1,2}, \hat{d}^k_{2,C} \rangle) < \theta_1$ or $\langle \hat{d}^k_{1,2}, \hat{d}^k_{2,C} \rangle \geq cos(\theta_1) = \beta_1$. As soon as the particles are aligned, the push maneuver is invoked.

One of the phenomena, that we observed when the alignment occurs is that of binding (Burns et al., 1989; Karásek et al., 2008). If the effector bead and the intermediate bead come too close to each other, they get binded partially due to optical force (known as optical binding) and also due to fluid and particle surface interaction. This leads to an undesirable situation in which when the effector bead rotates to align, the intermediate bead performs the same motion due to temporary binding with the effector bead. We solve the above problem by using a *backup* maneuver. Before applying the *align* maneuver, the feedback planner determines the distance between the effector and the intermediate bead. If it is lesser than a threshold β_2 then the *backup* maneuver is invoked. According to the *backup* maneuver, the trap is moved in the opposite direction to $d_{1,2}$, which leads to breaking the temporary mechanical bond between the effector and the intermediate bead in the bead formation.

The *align* maneuver is triggered when a misalignment is detected (i.e., $\langle \hat{d}^k_{1,2}, \hat{d}^k_{2,C} \rangle < \beta_1$). During the execution of the *align* maneuver, the trap T_1 moves along a circular arc (of the radius β_3) until the alignment occurs. When the inner product $\langle \hat{d}^k_{1,2}, \hat{d}^k_{2,C} \rangle$ becomes smaller than β_1, a waypoint is created at a distance of β_2 from the center of P_2 along

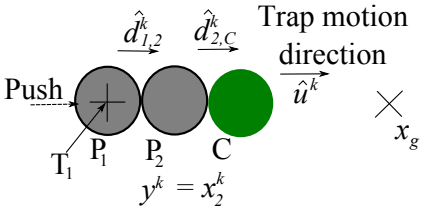

(a) Push: When the effector bead, intermediate bead, cell, and goal are all aligned then *push* is invoked.

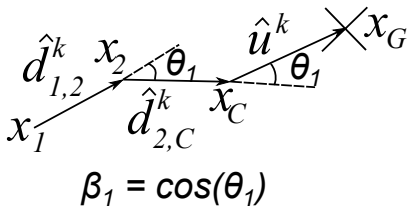

(b) Alignment of unit vectors $\hat{d}^k_{2,C}$, $\hat{d}^k_{1,2}$, and u^k.

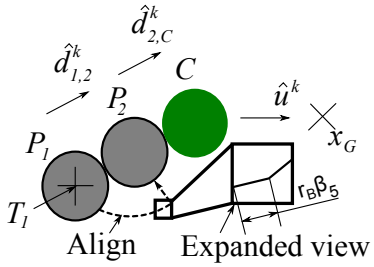

(c) Align: The bead P_1 is moved along the dotted line to its arrowhead so that the bead P_2 can be pushed to align it with the cell C and goal x_g. In one time step the bead moves $r_B\beta_5$ distance along a circular arc.

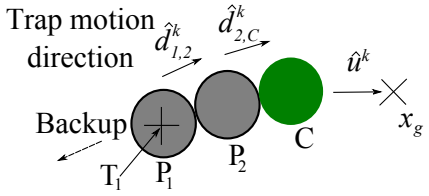

(d) Backup: When the distance between the beads P_1 and P_2 is less than the threshold β_2 then *backup* is invoked.

Figure 5: The maneuvers utilized by the feedback policy (P_1 and P_2 are the effector bead and intermediate bead of the bead formation, respectively, and C is the cell).

the normal of $\hat{d}_{2,C}$. The trap T_1 moves along the normal so that P_2 is pushed by P_1 for alignment. Let $\hat{u}^k = \frac{x_g - x_C^k}{\|x_g - x_C^k\|}$ be the unit vector along the direction between the cell and the goal location. Once the angle between $\hat{d}_{2,C}$ and the direction to the goal $\hat{u}^k$ is smaller than a given threshold β_4, a movement along a circular arc of radius β_5 is executed, otherwise the *push* maneuver is invoked. Depending upon the relative placement of the goal with respect to the other particles, the effector bead either needs to move clockwise or counterclockwise to place it suitably behind the intermediate bead (see Figure 6). The effector bead can then push the intermediate bead along an arc so that the intermediate bead, cell, and goal are all aligned. To determine the sense of movement of the effector bead, first α is determined as shown in Figure 6. After this, β is determined according to Algorithm 1. The term β is an intermediate quantity and hence is not shown graphically. The values of the threshold parameters $\beta_1, \beta_2, .., \beta_5$ depend upon the turning angle of the intended path of the cell. The above procedure is described in the Algorithm 1.

5.2 Parameter Optimization

One of the issues related to the use of the feedback policy presented in Algorithm 1 is the tuning of the parameters $\beta = [\beta_1, \beta_2, \beta_3, \beta_4, \beta_5]$. For various turning angles and noise levels to which an ensemble is subject to, the choice of the parameters β_j varies. Manual

Algorithm 1 LocalFeedbackPolicy

1: If P_1, P_2 and C are all aligned along the direction to the goal, i.e., $\langle \hat{d}^k_{1,2}, \hat{d}^k_{2,C} \rangle < \beta_1$ and $\langle \hat{d}^k_{2,C}, \hat{u}^k \rangle < \beta_1$, then $y^k = PUSH(S^k)$ and go to step 3, otherwise go to step 2.
2: If $\langle \hat{u}^k, \hat{d}_{2,C} \rangle < \beta_1$ and $\|x^k_1 - x^k_2\| < \beta_2$ then $y^k = BACKUP(S^k)$ else if $\langle \hat{u}^k, \hat{d}_{2,C} \rangle < \beta_1$ then $y^k = ALIGN(S^k)$. Here, $\epsilon > 0$ is a user defined small positive real number representing numerical tolerance.
3: Compute unit vector $\hat{u}^k_1 = \frac{y^k - x^k_1}{\|y^k - x^k_1\|}$.
4: Return $v^k_1 = s_{max} \hat{u}^k_1$.
5:
6: **procedure** PUSH(S^k, β)
7: Return $y^k = x^k_2$
8: **end procedure**
9:
10: **procedure** ALIGN(S^k, β)
11: Compute $\alpha = \langle (\hat{u}^k \times \hat{d}_{2,C}), [0, 0, 1]^T \rangle$.
12: Compute a normal vector $\hat{n}_{2,C}$ to $\hat{d}_{2,C}$ in the favorable direction so that the intermediate bead and the cell can be aligned to the goal direction using $\hat{n}_{2,C} = [\alpha \hat{d}_{2,C}(2), -\alpha \hat{d}_{2,C}(1), 0]^T$.
13: If $\langle \hat{d}_{2,C}, \hat{d}_{1,2} \rangle < \beta_3$ then return $y^k = x^k_1 + \beta_4 \hat{n}_{2,C}$ else go to step 14.
14: Compute $\gamma = \langle (\hat{d}_{1,2} \times \hat{n}_{2,C}), [0, 0, 1]^T \rangle$
15: Compute rotational angular increment $\Delta\theta = 0.05 \alpha \gamma$ and rotation matrix

$$R_{\Delta\theta} = \begin{pmatrix} cos(\Delta\theta) & -sin(\Delta\theta) & 0 \\ sin(\Delta\theta) & cos(\Delta\theta) & 0 \\ 0 & 0 & 1 \end{pmatrix}.$$

16: Return $y^k = x^k_2 - \beta_5 r_B R_{\Delta\theta} \hat{d}_{1,2}$
17: **end procedure**
18:
19: **procedure** BACKUP(S^k, β)
20: Return $y^k = x^k_2 - \beta_5 d_{1,2}$.
21: **end procedure**

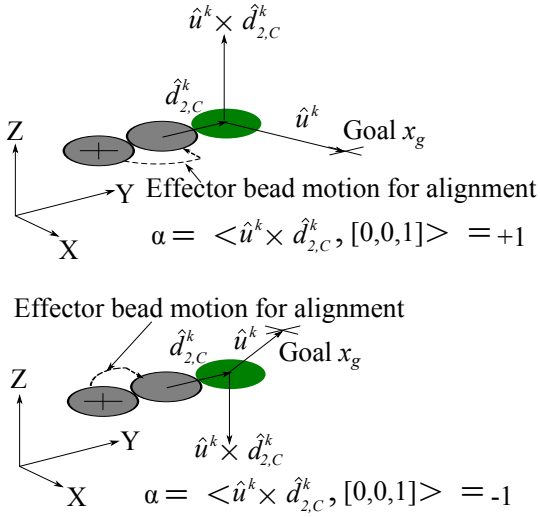

Figure 6: Motion control of the effector bead in response to the current state of the intermediate bead, cell, and the goal.

tuning of the parameters is a time consuming process and can be made more efficient by using an optimization technique. We present an automated parameter tuning approach based on the developed simulation and genetic algorithm (GA) based optimization.

To formulate the parameter tuning as an optimization problem, we chose the parameters β_j as design variables. The fitness function depends upon two factors, namely, (1) the time required for transporting an ensemble, and (2) the path following accuracy. To evaluate candidate sets of parameters, we generated multiple scenarios of paths with varying turning angles ranging from -90^o to 90^o with the increments of 30^o and the total path length of 40 μm. We chose the maximum trap speed to be 3 μm s^{-1}. The cell and bead diameter is taken as 5 μm. We simulated 5 different levels of sensor noise with fixed seeding for each scenario and then applied them in the simulation. We define the fitness function as

$$f(\beta, s_\theta) = \sum_{j=1}^{5} w_1 t_j + w_2 e_j \tag{8}$$

where t_j is the time required for transporting the cell and e_j is the deviation from the intended path computed using Algorithm 1, w_1 and w_2 are the weights, the index j is used for generating a seed for fixed pseudo-random noise generation, and s_θ is the path with the given turning angle θ.

We utilized Matlab^{TM} genetic algorithm toolbox for optimizing the parameters for each turning angle. We chose a population size of 200 and an uniform mutation with the probability of 0.03. We seeded the genetic algorithm with previously found solutions and successively improved the solutions until no further improvements were observed. We executed tests for 1000 different random measurement noise samples for each turning angle, in order to test the robustness of the planner with the optimized parameter values. We simulated the noise based on the covariance matrix determined in Section 4.2. The seeds for the random noise for each of 1000 cases are kept fixed for each test case, namely the turning angles. Variation of transportation time with respect to different turning angles is shown in Figure 7. The transportation time depends upon turning angle. In case of a large or steep turning angle, the ensemble needs to spend more time aligning

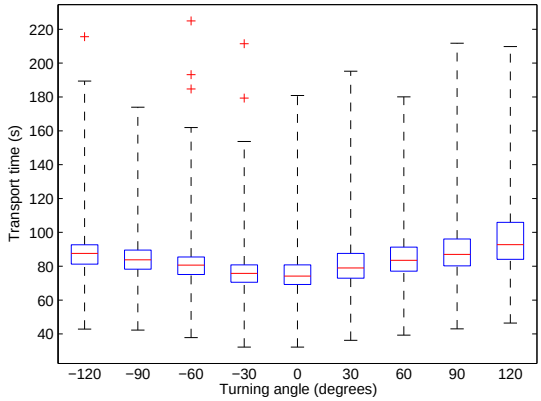

Figure 7: Optimized transport time of the ensemble under various turning angles and 1000 random measurement noise samples.

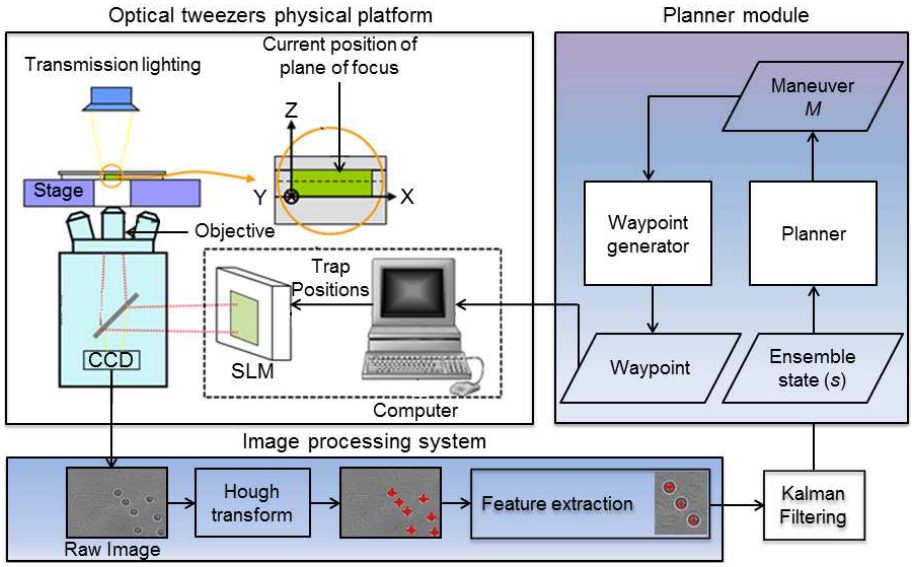

Figure 8: An overview of the experimental system.

with the goal, thereby increases the transportation time (see Figure 7).

For a large number of random measurement noises, the transport time does not deviate significantly (see Figure 7). This is an empirical evidence that optimized parameters are robust to the sensor noise.

6 Experimental Results

In this section, we present the details of the experimental setup we used for evaluation of the feedback planning approach discussed in this paper (see Figure 8). We used BioRyx 200 (Arryx, Inc., Chicago, IL) holographic laser tweezer. BioRyx 200 consists of a Nikon Eclipse TE 200 inverted microscope, a Spectra-Physics Nd-YAG laser (emitting green light of wavelength 532 nm), a spatial light modulator (SLM), and proprietary phase mask generation software running on a desktop PC. Nikon Plan Apo 60x/1.4 NA, DIC H oil-immersion objective is used. The maximum rate at which traps can be set is the update rate of the SLM, which is 15 Hz, and the minimum step size is 150 nm. The feedback control is achieved using a second PC equipped with a uEye camera (IDS, Inc.,

Cambridge, MA) for imaging the workspace and running the software for executing the planning algorithm. We use 5 μm diameter silica beads (with the density of 2000 kg/m^3 and the refractive index of 1.46), purchased from Bangs Laboratories, Inc., Fishers, IN) as the actuated as well as intermediate beads. We use yeast cells as sample for transporting using indirect pushing. The cells are approximately spherical, and their diameter ranges from 4 to 7 μm.

Figure 9 shows an indirect transport of a yeast cell by the proposed bead formation (a video of this experimental result can be found in Extension 1). The formation consists of an effector bead actuated by an optical trap, and an intermediate bead that is used to keep the laser trap far away from the cell. The intermediate bead is not trapped by the laser. The optical trap is controlled using the feedback planner described in this paper. The planner moves the effector bead to push the intermediate bead in the formation and thereby indirectly pushes the cell. This allows to transport the cell towards the desired goal location through the transfer of momentum. The goal location x_g is initially set to the first waypoint the cell needs to be transported to. Once the cell reaches the waypoint, x_g is set to the next waypoint. The workspace and the goal location are shown in Figure 9(a) with an ensemble containing the effector bead, intermediate bead, and a yeast cell that need to be transported. The feedback planner selects appropriate maneuvers as described in Algorithm 1 depending upon the state of the ensemble. The state of the ensemble is determined by an automated image processing algorithm based on Hough transform (Duda and Hart, 1972).

Often, the alignment of the ensemble is broken due to the Brownian motion and dynamical interaction between fluid and the beads (see Figure 9(c) and 9(i)). The planner uses the *align* maneuver to rotate the trap around the intermediate bead in order to position the effector bead on an axis connecting the cell, the intermediate bead, and the goal x_g (see Figure 9(b)).

Due to the effect of Van-der Waals forces and trapping forces (known as optical binding (Burns et al., 1989; Karásek et al., 2008)), the intermediate bead sometimes gets stuck to the effector bead in the bead formation (see Figure 10). The beads in the figure have a diameter of 5 μm. The bead on the left is trapped optically while the bead on the right is freely diffusing. The trapped bead is gradually moved towards the freely diffusing bead and eventually starts pushing it. As the trapped bead begins pushing the freely diffusing bead, the distance between them as determined by the image processing module is 4.6 μm. Ideally, in case of a perfectly planar motion, the distance between the beads during pushing should not be less than 5 μm (i.e., the sum of the radius of the pushing and pushed particles). However, in this case, the beads move in slightly different planes and thus the distance between them is further reduced. This reduced distance and Van-der Waals and optical forces cause the bead to further move in different planes. This effect can be seen in Figure 10c, where the image processing module measures the distance between the beads to be 3.3 μm. This eventually leads to a planning failure as the boundaries of the beads merge, which leads to difficulties in automatically recognizing the individual beads.

The planner developed in this paper can automatically predict this phenomenon by continuously checking the distance between the intermediate and effector beads. The planner utilizes the *backup* maneuver to detach the effector bead from the intermediate bead if the distance between them drops below a user-specified threshold in order to prevent the sticking phenomena (see Figure 9(d)).

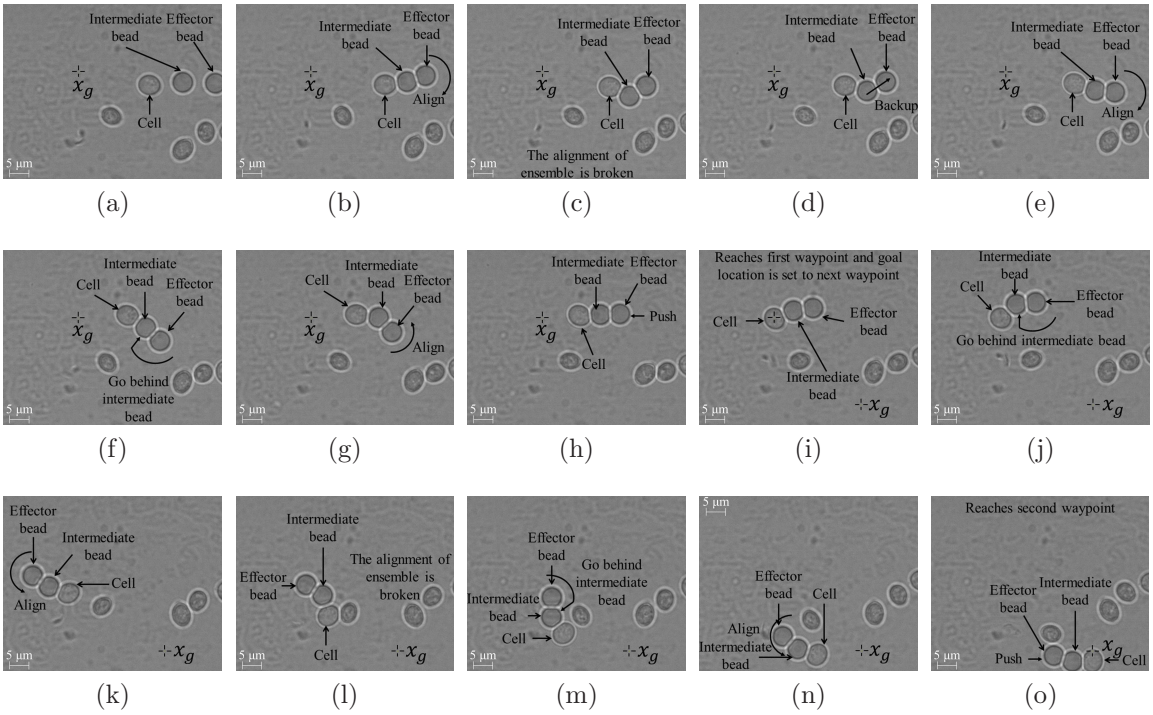

Figure 9: The experimental result of indirect pushing based transport of a target cell through multiple waypoints by the proposed bead formation. The formation is composed of an effector bead actuated by an optical trap and an intermediate bead used to protect the cell from a high intensity laser beam: (a) the initial state of the ensemble, (b) execution of the *align* maneuver to align the intermediate bead along the direction to the goal, (c) alignment of the ensemble is broken due to the dynamic fluid-particle interaction and Brownian motion, (d) execution of the *backup* maneuver to prevent sticking of the effector and intermediate beads due to Van-der Waals forces, (e) execution of the *align* maneuver to rotate the trap around the intermediate bead, (f) execution of the *align* maneuver to go behind the intermediate bead in order to align it towards the goal, (g) execution of the *align* maneuver to place the effector bead along the direction to the goal, (h) execution of the *push* maneuver to move the cell to reach the goal, (i) the ensemble reaches the first waypoint and the desired goal location is set to the next waypoint, (j) execution of the *align* maneuver to go behind the intermediate bead to re-align it towards the goal direction, (k) execution of the *align* maneuver to place the effector bead along the direction to the goal, (l) the alignment of the ensemble is broken due to the dynamic fluid-particle interaction and Brownian motion, (m) execution of the *align* maneuver to go behind the intermediate bead to align it towards the goal, (n) execution of the *align* maneuver to place the effector bead along the direction to the goal, and (o) the ensemble reaches the second waypoint with the use of the *push* maneuver.

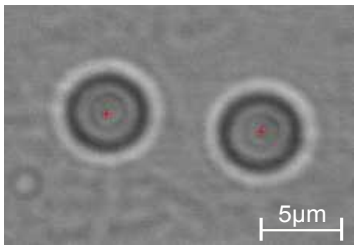

(a) The distance between the centers of the particles is 7 μm as detected by the image processing module and pushing has not yet started.

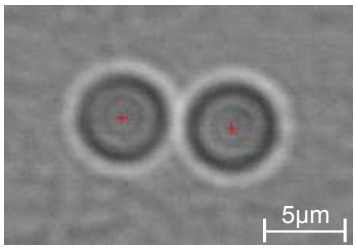

(b) The distance between the centers of the particles is 4.6 μm as detected by the image processing module and pushing has just started.

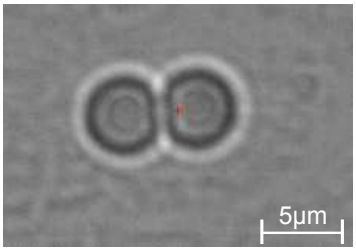

(c) The distance between the centers of the particles is 3.3 μm as detected by the image processing module and the particle boundary has disappered, making the detection of the centers of the beads to fail.

Figure 10: The particle on the left is optically trapped and pushes the freely diffusing particle on the right. The diameter of each particle is 5 μm. Due to the sticking phenomenon, the particles move in slightly different planes and the distance between them is observed to be 4.6 μm at the beginning of the *push* maneuver. As the pushing continues, the particles seem to get stuck to each other due to Van-der Waals and optical forces. These forces make the particles further slide into different planes, making the boundary between the two particles disappear.

The planner continues executing the maneuvers as soon as the effector bead moves to a safe distance from the intermediate bead (see Figures 9(e)– 9(g)) and until the ensemble gets aligned towards the goal. Finally, the planner executes the *push* maneuver to push the cell towards the goal (see Figure 9(h)).

Once the cell moves sufficiently close to the waypoint, the planner is assigned a new goal x_g represented as the next waypoint (see Figure 9(i)). The planner then continues executing suitable maneuvers until the cell reaches the final goal position (see Figures 9(j)–9(o)).

7 Conclusions

This paper presents a computational approach for performing an automated, image-guided, indirect micromanipulation of cells using a two-bead formation. The bead formation is composed of an optically actuated effector bead and a freely diffusing intermediate bead. The key components of the developed computational framework are the dynamics simulation of the indirect pushing, method for identification of the dynamics parameters and measurement noise, feedback planner that can handle sensor uncertainty in a robust manner, and optimization-based automated parameter tuning. We have experimentally demonstrated the application of the developed planning approach in a cell transport experiment using indirect pushing. The developed system can be utilized in biological experiments for studying cell migration, which is a fundamental process in metastasis and embryogenesis.

In the future, our aim is to carry out additional experiments under different operating conditions to further validate the robustness and flexibility of the developed approach. In particular, we will vary these conditions in terms of sensing uncertainties, fluid viscosi-

ties, laser power, and trap speeds. We would also like to generalize the feedback policy to deal with multiple effector and intermediate beads. This will allow us to automatically manipulate cells with more complex shapes. Irregular shaped cells as *Dictyostelium Discoideum* require a higher number of intermediate and effector beads for automated transport, which can be handled using a generalized framework consisting of several intermediate beads. We would also like to incorporate a global path planning algorithm in order to further optimize the motion of the ensemble. Finally, the heuristic cost function for the global planner can be precomputed by determining the transport time using the developed micromanipulation and simulation framework.

Funding

This research has been supported by NSF grants CMMI-0835572 and CPS-0931508. Opinions expressed are those of the authors and do not necessarily reflect opinions of the sponsors.

References

Aabo, T., Perch-Nielsen, I. R., Dam, J. S., Palima, D. Z., Siegumfeldt, H., Glckstad, J., and Arneborg, N. (2010). Effect of long- and short-term exposure to laser light at 1070nm on growth of saccharomyces cerevisiae. *Journal of Biomedical Optics*, 15(4):041505–041505–7.

Akella, S. and Mason, M. (1992). Posing polygonal objects in the plane by pushing. In *IEEE International Conference on Robotics and Automation (ICRA'92)*.

Ashkin, A. and Dziedzic, J. M. (1987). Optical trapping and manipulation of viruses and bacteria. *Science*, 235(4795):1517–1520.

Ashkin, A. and Dziedzic, J. M. (1989). Internal cell manipulation using infrared laser traps. *Proceedings of the National Academy of Sciences*, 86(20):7914–7918.

Ayano, S., Wakamoto, Y., Yamashita, S., and Yasuda, K. (2006). Quantitative measurement of damage caused by 1064-nm wavelength optical trapping of¡ i¿ escherichia coli¡/i¿ cells using on-chip single cell cultivation system. *Biochemical and biophysical research communications*, 350(3):678–684.

Banerjee, A. G., Balijepalli, A., Gupta, S. K., and LeBrun, T. W. (2009). Generating simplified trapping probability models from simulation of optical tweezers system. *Journal of Computing and Information Science in Engineering*, 9(2):1–9.

Banerjee, A. G., Chowdhury, S., Losert, W., and Gupta, S. K. (2011). Survey on indirect optical manipulation of cells, nucleic acids, and motor proteins. *Journal of Biomedical Optics*, 16(5):1–11.

Banerjee, A. G., Chowdhury, S., Losert, W., and Gupta, S. K. (2012). Real-time path planning for coordinated transport of multiple particles using optical tweezers. *IEEE Transactions on Automation Science and Engineering*, 9(4):669 –678.

Banerjee, A. G. and Gupta, S. K. (2013). Research in automated planning and control for micromanipulation. *IEEE Transactions on Automation Science and Engineering*, 10(3):485–495.

Banerjee, A. G., Pomerance, A., Losert, W., and Gupta, S. K. (2010). Developing a stochastic dynamic programming framework for optical tweezer-based automated particle transport operations. *IEEE Transactions on Automation Science and Engineering* , 7(2):218–227.

Behrens, M., Shoudong, H., and Dissanayake, G. (2010). Models for pushing objects with a mobile robot using single point contact. In *IEEE/RSJ International Conference on Intelligent Robots and Systems (IROS'10)*.

Bergeles, C., Shamaei, K., Abbott, J., and Nelson, B. (2010). Single-camera focus-based localization of intraocular devices. *Biomedical Engineering, IEEE Transactions on*, 57(8):2064 –2074.

Bista, S., Chowdhury, S., Gupta, S. K., and Varshney, A. (2013). Using GPUs for real-time prediction of optical forces on microsphere ensembles. *Journal of Computing and Information Science in Engineering*, 13(3):031002.

Bose, S., Singh, R., Hollatz, M. H., Lee, C. H., Karp, J., and Karnik, R. (2012). Microfluidic devices for label-free separation of cells through transient interaction with asymmetric receptor patterns. In *Bulletin of the American Physical Society*.

Burns, M. M., Fournier, J.-M., and Golovchenko, J. A. (1989). Optical binding. *Phys. Rev. Lett.*, 63:1233–1236.

Cappelleri, D. J., Fu, Z., and Fatovic, M. (2012). Caging for 2d and 3d micromanipulation. *Journal of Micro-Nano Mechatronics*, 7:115–129.

Chapin, S. C., Germain, V., and Dufresne, E. R. (2006). Automated trapping, assembly, and sorting with holographic optical tweezers. *Optics Express*, 14(26):13095–13100.

Chen, H., Wang, C., and Lou, Y. (2013). Flocking multiple microparticles with automatically controlled optical tweezers: Solutions and experiments. *Biomedical Engineering, IEEE Transactions on*, PP(99):1. Accepted for publication.

Chowdhury, S., Svec, P., Wang, C., Losert, W., and Gupta, S. (2012a). Gripper synthesis for indirect manipulation of cells using holographic optical tweezers. In *IEEE International Conference on Robotics and Automation (ICRA'12)*, pages 2749–2754. IEEE.

Chowdhury, S., Svec, P., Wang, C., Seale, K., Wikswo, J. P., Losert, W., and Gupta, S. K. (2011). Investigation of automated cell manipulation in optical tweezers-assisted microfluidic chamber using simulations. In *5th International Conference on Micro- and Nano Systems (MNS)*.

Chowdhury, S., Svec, P., Wang, C., Seale, K., Wikswo, J. P., Losert, W., and Gupta, S. K. (2012b). Automated cell transport in optical tweezers-assisted microfluidic chambers. *IEEE Transactions on Automation Science and Engineering*. Accepted for publication.

Chowdhury, S., Thakur, A., Wang, C., Svec, P., Losert, W., and Gupta, S. (2012c). Automated indirect transport of biological cells with optical tweezers using planar gripper formations. In *8th IEEE International Conference on Automation Science and Engineering*, pages 267–272. IEEE.

Chowdhury, S., Thakur, A., Wang, C., Svec, P., Losert, W., and Gupta, S. K. (2013). Automated manipulation of biological cells using gripper formations controlled by optical tweezers. *IEEE Transactions on Automation Science and Engineering*. Conditionally accepted for publication.

Cosgun, A., Hermans, T., Emeli, V., and Stilman, M. (2011). Push planning for object placement on cluttered table surfaces. In *IEEE/RSJ International Conference on Intelligent Robots and Systems (IROS'11)*.

Duda, R. O. and Hart, P. E. (1972). Use of the hough transformation to detect lines and curves in pictures. *Commun. ACM*, 15(1):11–15.

Ergeneman, O., Chatzipirpiridis, G., Pokki, J., Marín-Suárez, M., Sotiriou, G., Medina-Rodríguez, S., Sánchez, J., Fernández-Gutiérrez, A., Pané, S., and Nelson, B. (2012). In vitro oxygen sensing using intraocular microrobots. *Biomedical Engineering, IEEE Transactions on*, 59(11):3104 –3109.

Frutiger, D. R., Vollmers, K., Kratochvil, B. E., and Nelson, B. J. (2009). Small, fast, and under control: Wireless resonant magnetic micro-agents. *The International Journal of Robotics Research*.

Gossett, D., Weaver, W., Mach, A., Hur, S., Tse, H., Lee, W., Amini, H., and Di Carlo, D. (2010). Label-free cell separation and sorting in microfluidic systems. *Analytical and Bioanalytical Chemistry*, 397:3249–3267. 10.1007/s00216-010-3721-9.

Graydon, O. (2011). Optical manipulation: Tweezer app for iPad. *Nature Photonics*, 5(5):255.

Hu, S. and Sun, D. (2011). Automatic transportation of biological cells with a robot-tweezer manipulation system. *The International Journal of Robotics Research*, 30(14):1681–1694.

Igarashi, T., Kamiyama, Y., and Inami, M. (2010). A dipole field for object delivery by pushing on a flat surface. In *IEEE International Conference on Robotics and Automation (ICRA'10)*.

Ingber, D. E. (2006). Mechanical control of tissue morphogenesis during embryological development. *The International journal of developmental biology*, 50(2-3):255–266.

Karásek, V., Čižmár, T., Brzobohatý, O., Zemánek, P., Garcés-Chávez, V., and Dholakia, K. (2008). Long-range one-dimensional longitudinal optical binding. *Phys. Rev. Lett.*, 101:143601.

Konig, K., Liang, H., Berns, M. W., and Tromberg, B. J. (1995). Cell-damage by near-in microbeams. *Nature*, 377(6544):20–21.

Konig, K., Svaasand, L., Liu, Y. G., Sonek, G., Patrizio, P., Tadir, Y., Berns, M. W., and Tromberg, B. J. (1996). Determination of motility forces of human spermatozoa using an 800 nm optical trap. *Cellular and Molecular Biology*, 42(4):501–509.

Kopicki, M., Wyatt, J., and Stolkin, R. (2009). Prediction learning in robotic pushing manipulation. In *International Conference on Advanced Robotics (ICAR'09)*.

Koss, B., Chowdhury, S., Aabo, T., Gupta, S. K., and Losert, W. (2011). Indirect optical gripping with triplet traps. *Journal of the Optical Society of America B*, 28(5):982–985.

Landolsi, F., Ghorbel, F., and Dick, A. (2012). Analysis of the occurrence of stick-slip in afm-based nano-pushing. *Nonlinear Dynamics*, 68:177–186.

LaValle, S. M. (2006). *Planning algorithms*. Cambridge University Press, Cambridge, U.K. Available at http://planning.cs.uiuc.edu/.

Leach, J., Wulff, K., Sinclair, G., Jordan, P., Courtial, J., Thomson, L., Gibson, G., Karunwi, K., Cooper, J., Laczik, Z. J., and Padgett, M. (2006). Interactive approach to optical tweezers control. *Applied Optics*, 45(5):897–903.

Li, Q. and Payandeh, S. (2007). Manipulation of convex objects via two-agent point-contact push. *The International Journal of Robotics Research*, 26(4):377–403.

Liu, Y., Sonek, G. J., Berns, M. W., and Tromberg, B. J. (1996). Physiological monitoring of optically trapped cells: Assessing the effects of confinement by 1064-nm laser tweezers using microfluorometry. *Biophysics Journal*, 71(4):2158–2167.

Lynch, K. (1999). Locally controllable manipulation by stable pushing. *IEEE Transactions on Robotics and Automation*, 15(2):318 –327.

Mason, M. T. (1986). Mechanics and planning of manipulator pushing operations. *The International Journal of Robotics Research*, 5(3):53–71.

McNerney, G. P., Hubner, W., Chen, B. K., and Huser, T. (2010). Manipulating CD4+ T cells by optical tweezers for the initiation of cell-cell transfer of HIV-1. *Journal of Biophotonics*, 3(4):216–223.

Neuman, K. C., Chadd, E. H., Liou, G. F., Bergman, K., and Block, S. M. (1999). Characterization of photodamage to escherichia coli in optical traps. *Biophysics Journal*, 77(5):2856–2863.

Neuman, K. C. and Nagy, A. (2008). Single-molecule force spectroscopy: optical tweezers, magnetic tweezers and atomic force microscopy. *Nature Methods*, 5(6):491–505.

Pawashe, C., Floyd, S., and Sitti, M. (2009). Modeling and experimental characterization of an untethered magnetic micro-robot. *The International Journal of Robotics Research*.

Pereira, G. A. S., Campos, M. F. M., and Kumar, V. (2004). Decentralized algorithms for multi-robot manipulation via caging. *The International Journal of Robotics Research*, 23(7-8):783–795.

Rasmussen, M. B., Oddershede, L. B., and Siegumfeldt, H. (2008). Optical tweezers cause physiological damage to escherichia coli and listeria bacteria. *Applied and environmental microbiology*, 74(8):2441–2446.

Rezzoug, N. and Gorce, P. (1999). Dynamic control of pushing operations. *Robotica*, 17(06):613–620.

Sakaki, K., Dechev, N., Burke, R., and Park, E. (2009). Development of an autonomous biological cell manipulator with single-cell electroporation and visual servoing capabilities. *Biomedical Engineering, IEEE Transactions on*, 56(8):2064 –2074.

Schriebl, K., Satianegara, G., Hwang, A., Tan, H. L., Fong, W. J., Yang, H. H., Jungbauer, A., and Choo, A. (2012). Selective removal of undifferentiated human embryonic stem cells using magnetic activated cell sorting followed by a cytotoxic antibody. *Tissue Engineering Part A*, pages 899–909.

Shojaei-Baghini, E., Zheng, Y., and Sun, Y. (2013). Automated micropipette aspiration of single cells. *Annals of Biomedical Engineering*, pages 1–9.

Sims, N. R. and Anderson, M. F. (2008). Isolation of mitochondria from rat brain using Percoll density gradient centrifugation. *Nature Protocols*, 3(7):1228–1239.

Singer, W., Bernet, S., and Ritsch-Marte, M. (2001). 3D-force calibration of optical tweezers for mechanical stimulation of surfactant-releasing lung cells. *LASER PHYSICS*, 11(11):1217–1223.

Steager, E. B., Selman Sakar, M., Magee, C., Kennedy, M., Cowley, A., and Kumar, V. (2013). Automated biomanipulation of single cells using magnetic microrobots. *The International Journal of Robotics Research*, 32(3):346–359.

Svoboda, K. and Block, S. M. (1994). Biological applications of optical forces. *Annual Review of Biophysics Biomolecular Structure*, 23:247–285.

Tan, Y., Sun, D., Wang, J., and Huang, W. (2010). Mechanical characterization of human red blood cells under different osmotic conditions by robotic manipulation with optical tweezers. *IEEE Transactions on Biomedical Engineering*, 57(7):1816 –1825.

Tavalaee, M., Deemeh, M., Arbabian, M., and Nasr-Esfahani, M. (2012). Density gradient centrifugation before or after magnetic-activated cell sorting: which technique is more useful for clinical sperm selection? *Journal of Assisted Reproduction and Genetics*, 29:31–38. 10.1007/s10815-011-9686-6.

Thakur, A., Chowdhury, S., Svec, P., Wang, C., Losert, W., and Gupta, S. (2012). Automated indirect optical micromanipulation of biological cells using indirect pushing to minimize photo-damage. In *ASME 2012 International Design Engineering Technical Conference (IDETC) & Computers and Information in Engineering Conference (CIE), Chicago, IL*.

Vedula, S. R. K., Leong, M. C., Lai, T. L., Hersen, P., Kabla, A. J., Lim, C. T., and Ladoux, B. (2012). Emerging modes of collective cell migration induced by geometrical constraints. *Proceedings of the National Academy of Sciences*.

Wang, C., Chowdhury, S., Gupta, S. K., and Losert, W. (2013). Optical micromanipulation of active cells with minimal perturbations: direct and indirect pushing. *Journal of Biomedical Optics*, 18(4):045001.

Weijer, C. J. (2009). Collective cell migration in development. *Journal of Cell Science*, 122(18):3215–3223.

Wu, Y., Dong, S., and Wenhao, H. (2011). Force and motion analysis for automated cell transportation with optical tweezers. In *9th World Congress on Intelligent Control and Automation (WCICA'11)*.

Wu, Y., Sun, D., Huang, W., and Xi, N. (2013). Dynamics analysis and motion planning for automated cell transportation with optical tweezers. *IEEE/ASME Transactions on Mechatronics*, 18(2):706–713.

Wu, Y., Tan, Y., Sun, D., and Huang, W. (2010). Force analysis and path planning of the trapped cell in robotic manipulation with optical tweezers. In *IEEE International Conference on Robotics and Automation (ICRA'10)*.

Xie, C., Chen, D., and Li, Y. (2005). Raman sorting and identification of single living micro-organisms with optical tweezers. *Optics Letters*, 30(14):1800–1802.

Yim, S., Goyal, K., and Sitti, M. (2013). Magnetically actuated soft capsule with the multimodal drug release function. *Mechatronics, IEEE/ASME Transactions on*, PP(99):1 –5. Accepted for publication.

Zhang, X. P., Leung, C., Lu, Z., Esfandiari, N., Casper, R. F., and Sun, Y. (2012). Controlled aspiration and positioning of biological cells in a micropipette. *Biomedical Engineering, IEEE Transactions on*, 59(4):1032 –1040.

Appendix A Index to Multimedia Extensions

Table of Multimedia Extensions

Extension	Media Type	Description
1	Video	Automated Indirect Pushing of a Yeast Cell